NeuroImage: Clinical 13 (2017) 154–163

Contents lists available at ScienceDirect

NeuroImage: Clinical

journal homepage: www.elsevier.com/locate/ynicl

9.4 T MR microscopy of the substantia nigra with pathological validation in controls and disease

LA Massey[a,b,*], MA Miranda[c], O Al-Helli[a,e], HG Parkes[e], JS Thornton[f], P-W So[g], MJ White[f], L Mancini[f], C Strand[b], J Holton[b], AJ Lees[a,b,d], T Revesz[b], TA Yousry[e,f]

[a]Sara Koe Progressive Supranuclear Palsy Research Centre, UCL Institute of Neurology, London, United Kingdom
[b]Queen Square Brain Bank for Neurological Disorders, Department of Molecular Neuroscience, UCL Institute of Neurology, London, United Kingdom
[c]Division of Radiology, Department of Medicine, School of Medicine, University of Panama, Panama City, Panama
[d]Reta Lila Weston Institute of Neurological Studies, UCL Institute of Neurology, London, United Kingdom
[e]Department of Brain Repair and Rehabilitation, UCL Institute of Neurology, London, United Kingdom
[f]Lysholm Department of Neuroradiology, National Hospital for Neurology and Neurosurgery, Queen Square, London, United Kingdom
[g]Institute of Psychiatry, Psychology and Neuroscience, King's College, University of London, London, United Kingdom

ARTICLE INFO

Article history:
Received 12 September 2016
Received in revised form 14 November 2016
Accepted 16 November 2016
Available online 17 November 2016

ABSTRACT

Background: The anatomy of the substantia nigra on conventional MRI is controversial. Even using histological techniques it is difficult to delineate with certainty from surrounding structures. We sought to define the anatomy of the SN using high field spin-echo MRI of pathological material in which we could study the anatomy in detail to corroborate our MRI findings in controls and Parkinson's disease and progressive supranuclear palsy.
Methods: 23 brains were selected from the Queen Square Brain Bank (10 controls, 8 progressive supranuclear palsy, 5 Parkinson's disease) and imaged using high field 9.4 Tesla spin-echo MRI. Subsequently brains were cut and stained with Luxol fast blue, Perls stain, and immunohistochemistry for substance P and calbindin. Once the anatomy was defined on histology the dimensions and volume of the substantia nigra were determined on high field magnetic resonance images.
Results: The anterior border of the substantia nigra was defined by the crus cerebri. In the medial half it was less distinct due to the deposition of iron and the interdigitation of white matter and the substantia nigra. The posterior border was flanked by white matter bridging the red nucleus and substantia nigra and seen as hypointense on spin-echo magnetic resonance images. Within the substantia nigra high signal structures corresponded to confirmed nigrosomes. These were still evident in Parkinson's disease but not in progressive supranuclear palsy. The volume and dimensions of the substantia nigra were similar in Parkinson's disease and controls, but reduced in progressive supranuclear palsy.
Conclusions: We present a histologically validated anatomical description of the substantia nigra on high field spin-echo high resolution magnetic resonance images and were able to delineate all five nigrosomes. In accordance with the pathological literature we did not observe changes in the nigrosome structure as manifest by volume or signal characteristics within the substantia nigra in Parkinson's disease whereas in progressive supranuclear palsy there was microarchitectural destruction.

1. Introduction

The substantia nigra (SN) is located in the mesencephalon posterior to the crus cerebri (CC) and anterior to the midbrain tegmentum and comprised of two anatomically and functionally distinct parts: the inferior and posterior SN *pars compacta* (SNc) containing pigmented melanised neurons, and the superior and anterior (ventral) SN *pars reticulata* (SNr). The dopaminergic neurons of the pars compacta project *via* the nigrostriatal pathway to the striatum, and there is a reciprocal striatonigral projection. The neurons of the SNr form one of the output nuclei of the basal ganglia which along with the internal segment of the globus pallidus project to the thalamus (Nieuwenhuys et al., 1988).

The striatonigral projection is commonly used to define the borders of the SN by staining for substance P (SP) (Gibb, 1992; Mai et al., 1986; McRitchie et al., 1995; McRitchie et al., 1996) or calbindin (CB) (McRitchie et al., 1996; Damier et al., 1999a, b; McRitchie and Halliday, 1995). Both antibodies label the neuropil and fibres within the SN rather than cell bodies with less immunoreactivity around

* Corresponding author at: Sara Koe Progressive Supranuclear Palsy Research Centre, UCL Institute of Neurology, London, United Kingdom.
E-mail address: lukemassey@doctors.net.uk (L.A. Massey).

http://dx.doi.org/10.1016/j.nicl.2016.11.015

clusters of pigmented cells (McRitchie et al., 1996; Damier et al., 1999a, b). Calbindin staining is more intensely medially where occasional positive neurons within the SNc may be found (McRitchie and Halliday, 1995).

The internal anatomy of the SN is complex and various divisions based on identifiable nuclear groups have been proposed (Gibb, 1992; McRitchie et al., 1995; McRitchie et al., 1996; Damier et al., 1999a, b; German et al., 1989; Fearnley and Lees, 1991; Gibb and Lees, 1991; Hassler, 1937; Olzewski, 1954). Although 60% of pigmented neurons reside in the matrix these are sparsely distributed relative to the 40% of densely packed neurons within well-defined 'nigrosomes' (Damier et al., 1999a). Nigrosome structure is maintained in the presence of Parkinson's disease pathology (Damier et al., 1999b) but the ventrolateral tier, or nigrosome 1 is most susceptible to neuronal loss in Parkinson's disease (German et al., 1989; Damier et al., 1999b; Fearnley and Lees, 1990; Hassler, 1938). Other neuronal groups may be affected by age (dorsolateral tier, N4) and other neurodegenerative diseases such as progressive supranuclear palsy (ventromedial tier) (Fearnley and Lees, 1991).

The anatomy of the SN on conventional MRI is not well defined (Adachi et al., 1999; Gorell et al., 1995; Martin et al., 2008; Savoiardo et al., 1994; Massey and Yousry, 2010). However, using high field MRI the SN is more clearly demarcated (Cho et al., 2011; Kwon et al., 2012), and nigrosome 1 is visible in the dorsolateral substantia nigra (Blazejewska et al., 2013) as the "swallow tail sign" which is lost in Parkinson's disease (Schwarz et al., 2014) and other parkinsonian conditions (Reiter et al., 2015).

Clinicopathological studies confirm that even in the most experienced hands Parkinson's disease and progressive supranuclear palsy can be difficult to diagnose accurately and reliable biomarkers are an unmet need. The aim of this study was to produce an accurate, validated and detailed description of the anatomy of the SN based on histological staining including immunohistochemistry and Perls stain of the same tissue studied with high field spin-echo MRI at 9.4 Tesla – so called *MR microscopy* - and describe anatomical changes based on histological findings in disease including Parkinson's disease and progressive supranuclear palsy.

2. Materials and methods

Post-mortem brain tissue was obtained from the Queen Square Brain Bank for Neurological Disorders (QSBB), UCL Institute of Neurology, where tissue is donated according to ethically approved protocols and is stored under a licence from the Human Tissue Authority. Brains were sampled for histology using an established protocol (Trojanowski and Revesz, 2007) and the diagnosis confirmed using standard neuropathological criteria (Ince et al., 2008).

2.1. Tissue preparation

Formalin-fixed tissue was dissected to produce a tissue block to include the upper pons, entire midbrain with the substantia nigra and ventral diencephalon. The MRI axis was aligned perpendicular to the long axis of the brainstem and, after imaging the specimen was sliced in approximately 5 mm thick tissue blocks along this midline sagittal axis which were subsequently embedded in paraffin wax.

2.2. MRI protocol

Samples were imaged at room temperature in *perfluoropolyether* (Fomblin, Solvay Selexis) at 9.4 T (Varian NMRS MRI) with a 40 mm quadrature volume RF coil as previously described (Massey et al., 2012b).

1. Parameters for high-resolution spin-echo (SE) images were: TE 15–22 ms, TR 2000–2200 ms, scan averages 24–32, interleaved slices, slice thickness 0.5–1 mm, slice gap 0.5–1 mm, matrix 512 × 512, field of view (FOV) 45 × 45 mm (in-plane resolution 88 μm) and imaging time up to 10 h.
2. Superior in-plane resolution was obtained in one case: 1024 × 1024 matrix (in plane resolution 44 μm), 132 averages; other parameters as above, imaging time 72 h.

These parameters were chosen on the basis of pilot acquisitions to yield optimal image contrast for the structures of interest. Images were viewed and processed in ImageJ (version 1.43h, US National Institutes of Health, Bethesda, Maryland) (Rasbrand, 2009).

2.3. Histological protocol

The paraffin wax embedded tissue blocks were serially sectioned at 20 μm. Every 20th section was stained with the Luxol fast blue and Cresyl Violet (LFB/CV) method. MRI images and LFB/CV stained slides were visually compared and once the best match between histology and MRI was identified, neighbouring tissue sections were stained with Perls stain for iron and used for immunohistochemistry with antibodies to substance P (SP) and calbindin (CB). For immunohistochemistry sections were dewaxed, taken to absolute alcohol and blocked in H_2O_2/methanol. For substance P immunohistochemistry tissue sections were blocked in 10% normal swine serum for 10 min. Tissue sections were incubated with the primary antibodies for 1 h at room temperature and then washed in PBS. Polyclonal antibodies were incubated in swine anti rabbit 1:200 for 30 mins. Monoclonal antibodies were incubated in rabbit anti mouse 1:200 for 30 mins and then washed in PBS. All sections were incubated in Vector ABC for 30 mins and washed in PBS. The colour was developed with glucose oxidase nickel dab solution. Sections were counterstained in Mayer's haematoxylin and washed dehydrated and mounted. The following antibodies were used: substance P (Invitrogen Polyclonal; 1:50); calbindin (Abcam Monoclonal; 1:400). Macroscopic images were obtained at 20–40× magnification using Image Pro Plus (Mediacybernetics, Bethesda, MD www.mediacy.com) and microscopic images using Leica biosystems digital image hub.

2.4. Image segmentation

MR images were segmented manually in ITK-SNAP (version 1.8.0) (Yushkevich et al., 2006). Reconstructions were made using the mesh function, and measurement of volume was performed on manually segmented regions. Linear measurements of SN breadth and width were performed in Image J.

2.5. Analysis

The anatomy of the SN was demonstrated in a single case with LFB/CV, Perls stain, SP and CB immunohistochemistry and high field SE MR microscopy at multiple serial axial levels through the SN. The anatomy was defined by overlying LFB/CV, SP, CB, Perls and SE MRI images level by level. A cartoon of the anatomy was developed to confirm the borders and internal anatomy of the SN. Once the anatomy was demonstrated the volume, dimensions and variability in borders, landmarks and internal anatomy was studied in control and disease cases (Parkinson's disease, progressive supranuclear palsy) at the level of the exit of the IIIrd cranial nerve and RN which is the most studied level in the pathological and radiological literature.

3. Results

3.1. Characteristics of cases studies

Twenty three cases were included in the study including 10 controls, 8 progressive supranuclear palsy and 5 Parkinson's disease [Table 1].

Table 1
Characteristics of cases imaged using high field MR microscopy.

No	Gender	Side fixed	Age	DOF (days)	Category	Pathological diagnosis
1	F	Both	94	4149	Control	n/a
2[a]	M	right	94	51	Control	Small vessel disease (severe), Braak & Braak stage IV
3[a]	M	right	38	56	Control	Minimal abeta deposition
4[a]	M	left	78	78	Control	CAA (moderate)
5	M	both	79	1029	Control	Pathological ageing, mild cvd
6	F	Left	82	366	Control	Pathological ageing, mild svd, mod CAA
7	F	Right	82	302	Control	Pathological ageing, right parietal infarct
8	F	Right	72	67	Control	MND
9	F	Right	99	26	Control	B&B IV NFT pathology
10	M	Left	89	18	Control	n/a
11[a]	M	Left	68	54	PSP	PSP, Lewy body pathology, pathological ageing
12[a]	M	Right	69	89	PSP	PSP, pathological ageing
13	M	Right	66	315	PSP	PSP
14	M	Right	86	165	PSP	PSP, pathological ageing, small haemorrhagic frontal focus
15	M	Whole	68	88	PSP	PSP, pathological ageing
16	M	Right	71	51	PSP	PSP
17	F	Right	75	85	PSP	PSP
18	M	Left	67	51	PSP	PSP, acute MCA infarct
19[a]	M	Left	79	260	PD	PD
20[a]	M	Right	83	28	PD	PD
21	M	Right	70	31	PD	PD, limbic Lewy body pathology
22	F	Left	62	45	PD	PD, neocortical Lewy body pathology
23	M	Left	71	31	PD	PD, limbic Lewy body pathology, neocortical Lewy body pathology, pathological ageing, mild CAA, focal hippocampal infarction

[a] These cases had Luxol fast blue, immunohistochemistry and Perl stain for comparison.

3.2. Defining the anatomy of the SN on SE MRI

The substantia nigra as defined by SP and CB immunohistochemistry was studied from the level of the STN [level 1] to the level of the brachium conjunctivum [level 7] in serial 0.5 mm thick axial sections spaced by 1.0 mm [Fig. 1A–E].

3.2.1. Borders

3.2.1.1. Anterior border. The anterior SN was bordered by the crus cerebri.

3.2.1.1.1. LFB/CV. The border was clear except superior and medially [Fig. 1B levels 1&2] where there were 'interdigitations' of blue-staining myelinated fibres and regions of low LFB/CV staining [Fig. 2A&B]. In the most medial portion there is white matter clustering which has the appearance of a 'hook' (see below) [Fig. 1B levels 2–4]. On the lateral border encroaching into the SN there is a myelinated cluster which has a triangular shape (anteromedial (AM) white matter see below) [Fig. 1B levels 2–5].

3.2.1.1.2. Perls. There is staining throughout the anterior border but particularly anteromedially [Fig. 1C all levels]. This encroached on the myelinated fibres of the corticospinal tracts and AM [Fig. 2B&E] (see below).

3.2.1.1.3. Immunohistochemistry. SP immunostain defines the anterior border by staining the striatonigral innervating fibres and is in agreement with the LFB/CV stain with fibres seen radiating into the CC [Figs. 1E, 2C&F]. This gives rise to a linear appearance which interdigitates with the crus cerebri [Fig. 1E levels 1–3]. CB also has a serrated appearance at this level but gives a more uniform appearance with denser staining medially.

3.2.1.1.4. Spin-echo MRI. The medial part of the anterior border is more diffuse but lacks the interdigitating/serrated appearance of the anatomical and immunocytochemistry [Fig. 1D levels 1–7]. There is a hypointense rim (HR) which corresponds to the anterior border but is more prominent superomedially.

3.2.1.2. Posterior border. The posterior border of the SN is somewhat controversial in the literature. Using SP immunohistochemistry the parabrachial nucleus (Halliday, 2004) or gamma group of Olzewski (Olzewski, 1954) are excluded and this definition has been used for this study.

3.2.1.2.1. LFB/CV. The posterior border is defined by myelinated fibres which appear to run in a posterolateral to anteromedial axis (Adachi et al., 1999; Gorell et al., 1995) seen at superior levels separating the SN from the STN [Fig. 1B level 1] or the RN/BC [Fig. 1B level 2–7]. Laterally at lower levels this is formed by the medial lemniscus (ML) which is more heavily myelinated [Fig. 1B level 6–7]. At mid-levels there is a small group of myelinated fibres which we have termed posterolateral white matter (PL) [Fig. 1B levels 2–5]. The medial posterior border is less clearly defined but at its most medial aspect is bounded by fibres of the third nerve in the mid-level section [Fig. 1B level 5].

3.2.1.2.2. Perls. At the most superior levels Perls stain for iron reveals dense staining on the medial posterior border [Fig. 1C level 1]. Below this relatively less iron is deposited in the posterior border than the anterior border of the SN [Fig. 1C levels 2–5] until at the lower levels there is more intense Perls staining particularly medially [Fig. 1C levels 6–7].

3.2.1.2.3. Immunohistochemistry. SP immunostain defines the border in correspondence with LFB/CV except in the mid levels lateral portion where there is a small posterior protrusion not seen on LFB/CV [Fig. 1E levels 3–4 arrowed]. CB stains as per LFB/CV although the medial-lateral gradient makes the lateral portion less evident.

3.2.1.2.4. Spin-echo MRI. At the most superior level a hypointense band (HB) separates the STN and SN [Fig. 1D level 1] (Massey et al., 2012a, b). At lower levels the border is defined by a high signal intensity band. At mid levels it is less clear and medially comprised of both a thin high intensity band adjacent to the RN a region of hypointensity bordering on the relative hyperintensity of the SN itself. At lower levels the hypointense band is more prominent corresponding to the increased Perls staining and the border is formed by a hyperintense band separating the SN from the ML laterally [Fig. 1C&D levels 6–7].

3.2.1.3. Lateral border

3.2.1.3.1. LFB/CV. The lateral border of the SN is bounded by the crus cerebri wrapping around the SN [Fig. 1B level 1–4] and the abutting of the CC and ML at lower levels [Fig. 1B level 5–7].

3.2.1.3.2. Perls. There is less iron staining at the most lateral portion of the border of the SN than medially but it is still evident at the most lateral portion.

3.2.1.3.3. Immunohistochemistry. The border is clearly defined although less so on CB than SP immunohistochemical preparation due to the medial-lateral gradient.

3.2.1.3.4. Spin-echo MRI. The border is clearly defined corresponding to the distribution of myelinated fibres with some iron on the anterior aspect of the lateral border.

3.2.1.4. Medial border. This is most clearly defined at the level of the exit of the fascicles of the third nerve.

3.2.1.4.1. LFB/CV. At levels where fascicles of the third nerve are found this defines the medial border [Fig. 1 level 5]. At other levels the medial border is determined by the medial edge of the tissue specimen.

3.2.1.4.2. Perls. The anterior medial SN has high iron staining.

3.2.1.4.3. Immunohistochemistry. These preparations clearly define a medial border.

3.2.1.4.4. Spin-echo MRI. The medial border is defined by a hyper intense rim formed by the bundles containing fascicles of the third nerve [Fig. 1 level 5].

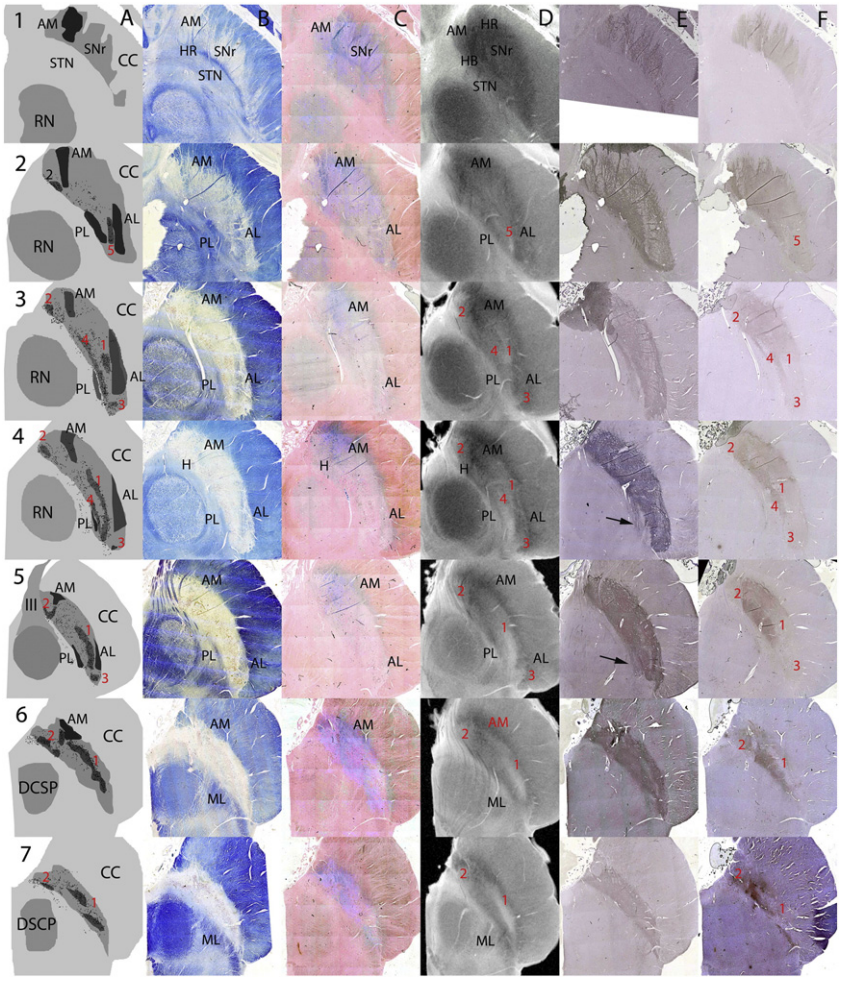

Fig. 1. The Anatomy of the SN on serial axial sections using Luxol fast blue/Cresyl Violet (LFB/CV), Perls stain, high field spin-echo MRI, and substance P (SP) and calbindin (CB) immunohistochemistry. Case 2 was a 36 yr old male. Serial axial sections at 1.5 mm through a single substantia nigra (SN) A: cartoon showing key anatomical structures based on SP and LFB/CV for borders, LFB/CV for location of pigmented neurons on substantia nigra pars compacta (SNc) and CB for nigrosomes. Pigmented neurons are shown as black dots and it is notable that not all of these fall within the CB-defined nigrosomes. B: LFB/CV. C: Perls stain. D: High field spin-echo MRI. E: SP. F: CB. Anatomical landmarks are in black. Nigrosomes (1–5) are labelled in red. See text for a detailed description of the anatomy and comparison of images.

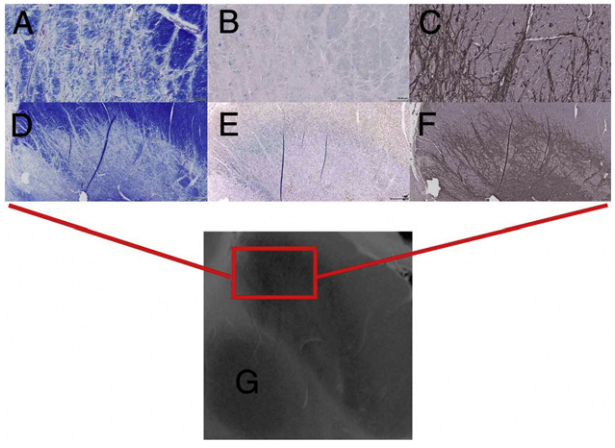

Fig. 2. The anteromedial border of the substantia nigra at superior levels. A–C 10× magnification; D–F 2× magnification. A & D Luxol fast blue/Cresyl Violet (LFB/CV), B & E Perls stain, C & F substance P (SP) immunohistochemistry. G High field spin-echo MRI image show region represented by histological sections. Lower and higher field histological sections using LFB/CV and SP show the interdigitation of white matter with the anteromedial border of the SN. Perls stain can be seen blurring the boundary of the SN in B & E and appears to stain both white matter in the border and within the anterior SN itself - the anteromedial white matter (AM) landmark - see text.

3.2.2. Three useful landmarks

We identified three internal landmarks within the SN:

1. Anterior Medial White Matter (AM): in the anterior and medial SN there are myelinated fibres appearing in the shape of a 'hook' (H) [Fig. 1A&B levels 1–6]. Clusters of fascicles of WM staining blue on LFB/CV and with Perls stain are seen within the SN indicating that they are a site of iron deposition. [Fig. 1C levels 1–6]. On spin-echo MRI there is corresponding signal hypointensity [Fig. 1D levels 1–6]. Higher field images demonstrate Perls staining as both pigment in the neuropil and in clusters of white matter [Fig. 2B&E].
2. Anterior Lateral White Matter (AL): in the anterolateral portion of the SN there is a triangular region containing myelinated fibres [Fig. 1B levels 2–5]. These fibres have higher Perls staining [Fig. 1C levels 2–5] and are seen as hypointense on MRI [Fig. 1D levels 2–5].
3. Posterior Lateral White Matter (PL): in the posterolateral SN there are myelinated fibres found just medial to the medial border of the SN [Fig. 1A&B levels 2–5]. At the most inferior levels these correspond to the medial lemniscus [Fig. 1B levels 6–7]. In contrast to the AL these do not appear to stain strongly for iron but are still signal hypointense [Fig. 1D levels 2–5] on SE MRI.

3.2.3. Substantia nigra pars reticularis (SNr)

The SNr was found anteriorly and superiorly to the SNc [Fig. 1A levels 1–3] and was thus more clearly visualised at superior levels -

pigmented cells were found from level 2–7 [Fig. 1A levels 2–7]. It is defined by non-pigmented cells on the LFB/CV preparation [Fig. 3]. It corresponds topographically to the region of strong iron staining anteriorly and medially at more superior levels [Fig. 1]. On high field spin-echo MRI it appears heterogeneously with a hypointense rim (HR) and relatively hyperintense core, and is not immediately distinguishable from the SNc using SP or CB immunohistochemistry or by signal characteristics on spin-echo MRI.

3.2.4. Substantia nigra pars compacta (SNc) internal anatomy

The SNc is defined by the presence of cells containing neuromelanin pigment [Fig. 1A all levels & Fig. 3]. These are visible on the LFB/CV and Perls stained sections and can be defined by location (Hassler, 1937; Gibb et al., 1990) or by using calbindin immunohistochemistry to delineate so-called 'nigrosomes' where there is relatively reduced calbindin staining of the neuropil (Damier et al., 1999a) [Fig. 1A&E levels 2–7; Fig. 3]. Not all pigmented cells are found in nigrosomes (Damier et al., 1999a) and this is demonstrated in the Cartoon [Fig. 1A levels 2–7]. On Perls stain there is less intense staining within the nigrosomes, particularly seen at lower levels [Fig. 1C levels 4–7] and Perls staining is less intense in nigrosomes [Fig. 1C level 6 & 7].

Nigrosome 1 (N1 - the 'ventrolateral tier') was seen in levels 3–7. It was closely apposed to the posterior border of AL [Fig. 1A&E levels 3–5] and formed a solitary band in lower levels [Fig. 1A&E levels 6–7]. On spin-echo MRI it appears as a hyperintense band radiating across from the posterolateral border towards the anteromedial border defined by hypointensity of the AL on the anterior border and a hypointense band on the posterior border particularly medially where the 'hook' formed by the AM was seen [Fig. 1A&D levels 3–7].

Nigrosome 2 (N2 - the pars medialis) was seen at all levels where pigmented cells were found [Fig. 1A&E levels 2–7] at the most posterior and medial tip of the SN. This was not so clearly seen on spin-echo MRI. There is relative signal hyperintensity at the most medial and posterior tip but this does not directly correspond to the size and shape of the region identified by calbindin immunohistochemistry, although the cluster of pigmented cells clearly extends beyond this region [Fig. 1A&E all levels].

Nigrosome 3 (N3 - the 'pars lateralis') was seen in levels 4–6. It is bounded by the AL and the CC as it wraps around the lateral border of the SN [Fig. 1A&B levels 3–5]. N3 was identified on spin-echo MRI by signal hyperintensity bounded by the low signal intensity of AL and the CC [Fig. 1A&D levels 3–5].

Nigrosome 4 (N4 - the 'dorsolateral tier') was seen in levels 3 & 4. It abutted the posterior border of the SN and the PL [Fig. 1 levels 3&4]. On spin-echo MRI it appeared as a hyperintense band posterior to N1 and bounded by the signal hypointensity of the parabrachial nucleus immediately adjacent.

Nigrosome 5 (N5) was found at the most superior level where pigmented cells were found only [Fig. 1A&E level 2]. This was seen on conventional MRI as a region of signal hyperintensity between the AL and PL.

On spin-echo MRI N1 and N4 in the lateral SNc give the appearance of a spin-echo signal hyperintense 'pincer' grasping a spin-echo signal hypointense 'hook' corresponding to the Perls staining AM.

3.2.5. Sagittal and coronal plane images

In case 8 sagittal and coronal high field MRI images were available. In the sagittal plane the superoposterior border of the SN is separated from the STN by a thin hypointense rim (HR); inferiorly spin-echo MRI hyperintense signal white matter separates it from the RN including the region of the parabrachial nucleus. The inferoanterior border of the SN abuts the CC along the entire length of the nucleus [Fig. 4A–H].

In the coronal plane the superomedial border is defined by a hypointense rim (HR) separating it from the STN in the superior half; in the inferior half it is separated from the RN by the spin-echo MRI hyperintense signal white matter. The inferolateral border is formed by the CC in the entire length of the SN [Fig. 4I–P].

3.2.6. Location, position and relations using spin-echo MRI

The SN was clearly identified in all 10 control cases studied (11 half brains). It was found in the anterior portion of the midbrain posterior to the CC and anterior to the STN, RN and DSCP. It lay at an oblique angle in all three planes: in the axial plane the SN was approximately 40° from the midline at the level of the STN and RN, and 30° at the level of the DSCP; on sagittal images it lay at 35° and in coronal images 45° with reference to the axis of the brainstem; on these latter two images the SN was seen to lie mostly inferior and lateral to the RN and encase the STN's inferolateral aspect.

3.3. Comparison of the SN between controls, Parkinson's disease and progressive supranuclear palsy

3.3.1. Volume and dimensions

The mean volume of the SN was 211.3 mm^3 in controls, 120.8 mm^3 in progressive supranuclear palsy and 180.8 mm^3 in Parkinson's disease. In progressive supranuclear palsy the volume was significantly reduced compared to controls ($p < 0.001$) and Parkinson's disease ($p = 0.008$), but there was no significant difference between Parkinson's disease and controls [Table 1]. The SN is most broad and deep at the level of the RN (mean width 11.72 mm; mean depth 2.99 mm), tapering at the superior extremity and resembling a tear in the sagittal and coronal planes [Fig. 4]. Maximal length in the sagittal plane was 14.0 mm and in the coronal plane 14.4 mm. In progressive supranuclear palsy depth at the level of the RN and DSCP and width at the level of the RN were reduced in progressive supranuclear palsy [Table 1] but not in Parkinson's disease.

3.3.2. Borders at the level of the RN

The anterior border was more clearly defined laterally with haziness in the medial section with heavy deposition of iron and WM, SP+ fibres

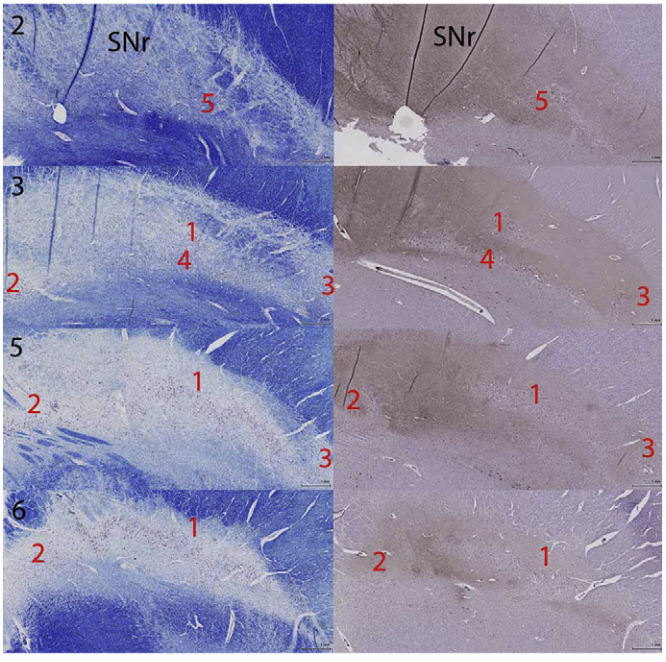

Fig. 3. The internal anatomy of the substantia nigra (SN) using Luxol fast blue/Cresyl Violet (LFB/CV) and calbindin (CB) immunohistochemistry. LFB/CV and CB stains delineating the anatomy of the nigrosomes within the SN at axial levels as per Fig. 1. At the superior level (2) anterior and medial SN represents a regions without neuromelanin containing neurons and is the substantia nigra pars reticulata (SNr). At the lower levels represented (3, 5, 6) clusters of neurons are seen both on LFB/CV and CB immunohistochemistry. On CB stain regions of relative CB-poor stain are designated nigrosomes (Damier et al., 1999a, b).

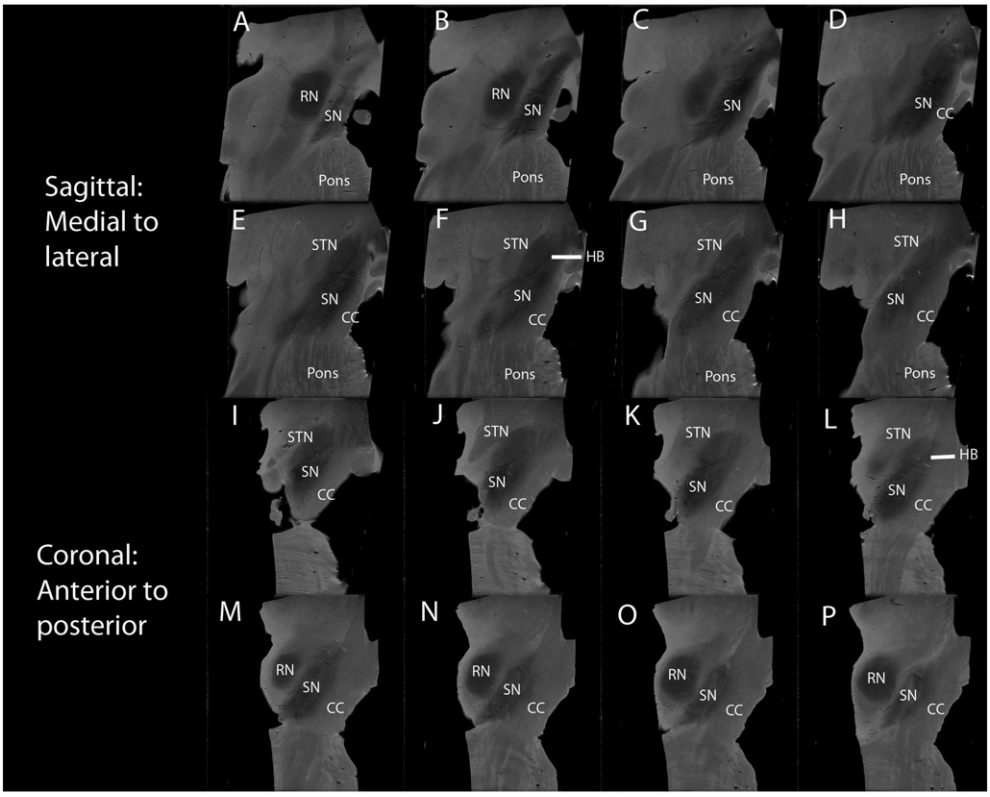

Fig. 4. Sagittal and coronal views using high field spin-echo MRI. A–H Serial sagittal views at 1 mm from medial to lateral. Substantia nigra (SN) inferior and anterior to the red nucleus (RN) medially, and to the subthalamic nucleus (STN) laterally. I–P Serial coronal views at 1 mm from anterior to posterior. The SN is inferior and tilted to the STN anteriorly and RN posteriorly. The crus cerebri (CC) forms the anterior border. Signal hypointensity is greater more medially (B–D) and anteriorly (I–L) within the SN. A hypointense band (HB) is seen separating the STN from the SN in both the sagittal (F) and coronal planes (L).

invaginating into the CC in controls, Parkinson's disease and progressive supranuclear palsy [Figs. 2, 5; Table 2]. This was also true on spin-echo MRI in controls and Parkinson's disease [Figs. 1, 5] although in progressive supranuclear palsy [Fig. 5] in some cases the lateral border was less distinct [Table 3].

The posterior border was defined by white matter of the PBN medially and laterally by PL on histology in control and disease cases [Table 2] and on spin-echo MRI [Table 3].

The medial border was clearly defined in all cases by fascicles of the IIIrd nerve and the medial CC and the lateral border was defined by the CC.

3.3.3. Landmarks at the level of the RN

AM, AL and PL were seen in all control and Parkinson's disease SNs at this level on histology and spin-echo MRI, but were less frequent in the progressive supranuclear palsy group, particularly PL which was only seen in 1/8 progressive supranuclear palsy SNs [Table 3].

3.3.4. Internal anatomy at the level of the RN

Overall and in keeping with the volume measurements [Table 1] the SN appears similar in controls and Parkinson's disease [Figs. 1, 5] but is markedly thinned in progressive supranuclear palsy [Fig. 5]. On histology N1, N3 and N4 were clearly visible and were associated with reduced Perls stain, whereas N2 was associated with increased Perls stain in controls. In the disease group the nigrosomes were much less densely populated with pigmented neurons in Parkinson's disease [Fig. 5] [Table 2]. In Parkinson's disease the nigrosomes looked thick and pale [Fig. 5]; in progressive supranuclear palsy thin and streaky with dense Perls staining [Fig. 5]. On spin-echo MRI, nigrosomes were paler in Parkinson's disease but still mostly identifiable [Fig. 5; Table 3], and in progressive supranuclear palsy were more difficult to identify and had a stringy/streaky appearance when seen [Fig. 5] [Table 3].

4. Discussion

We have demonstrated the anatomy of the SN using high field spin-echo MRI at 9.4 T and validated this by comparison with stained sections in the same post-mortem tissue. The anterior border of the SN was more clearly delineated laterally and inferiorly whereas there is blurring of the margins between the SN and CC, particularly anteriorly and medially at the most superior levels characterised by higher iron deposition on Perls staining and a serrated edge on SP immunohistochemistry. The posterior border is formed by white matter lying between the SN and RN in the medial aspect and the SL and ML in the lateral aspect and is mostly hypointense. The hyperintense band described in the literature is more posterior, abutting the RN and forms part of the PBN [Fig. 1B&D levels 3–5]. We have also described three white matter bundles defined by their anatomical position (AM, AL and PL) which are seen on high field MRI and are useful landmarks in the SN.

Within the SN itself there is heterogeneous signal. The region of the SNr is hypointense on spin-echo MRI with a hypointense rim defining its anterior border, and a hypointense band defining its posterior border from the STN. By using immunohistochemistry for CB we are able to accurately locate Damier's nigrosomes (Damier et al., 1999a). These are seen on high field spin-echo MRI as hyperintense regions whose position can be clarified by reference to the white matter landmarks AM, AL and PL. In controls the AM white matter landmark forms a hypointense hook appearance, and the combination of high signal from N1 and N4 at the level of the RN and IIIrd nerve fascicles gives a hyperintense 'pincer' appearance - similar to the 'swallow tail' appearance described using SWI *in vivo* (Schwarz et al., 2014) - which is bordered by the relatively hypointense AL white matter dorsally to N1. Perls stain confirms that the nigrosomes are relatively low in iron compared the immediate environs [Fig. 1] (Blazejewska et al., 2013).

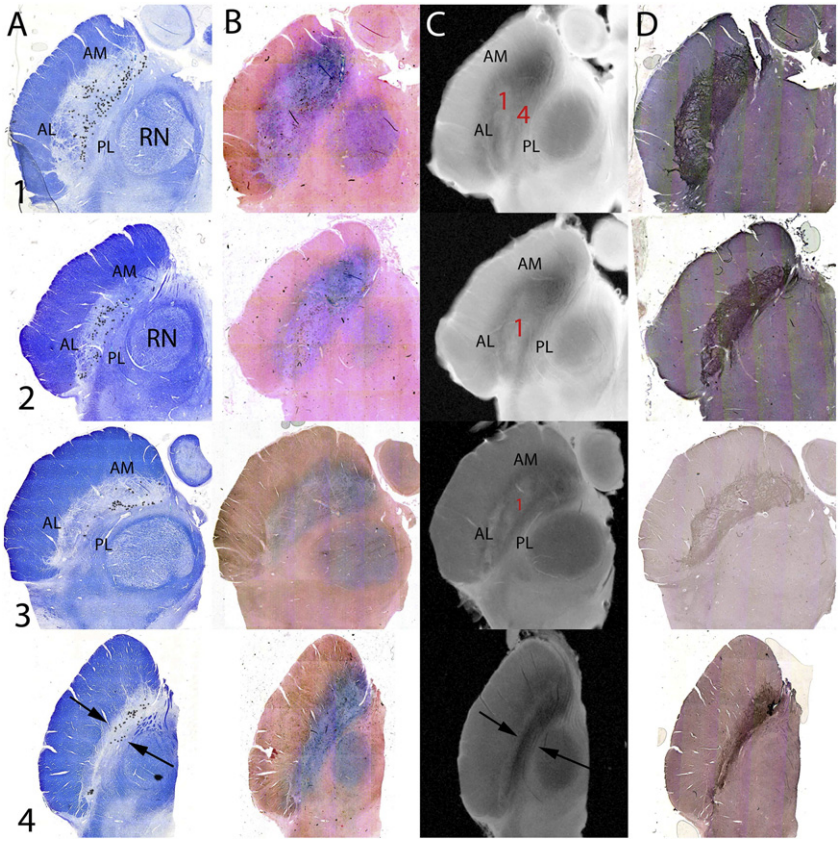

Fig. 5. The anatomy of the SN in control, Parkinson's disease and progressive supranuclear palsy cases: A: Luxol fast blue/Cresyl Violet (LFB/CV). B: Perls stain. C: High field spin-echo MRI. D: Substance P (SP) immunohistochemistry. [1] 94 yr old control male just above the exit of the IIIrd nerve. [2] 94 yr old control male at the level of the exit of the IIIrd nerve fascicles. The pigmented neurons of nigrosome 1 (N1) are clearly seen within a region of reduced Perls staining and as a hyperintense band on Spin-Echo MRI. The pincer and hook are clearly visualised, and the white matter landmarks (anteromedial) AM, (anterolateral) AL and (posterolateral) PL. [3] 79 yr old male with Parkinson's disease. Borders and white matter landmarks are present and subjectively and objectively does not appear to have lost volume [Table 2]. Spin-echo MRI shows a high intensity band consistent with N1 when compared with control images. However, the remaining neuromelanin containing neurons are not within this structure. [4] 68 yr old male with progressive supranuclear palsy. The whole structure is markedly atrophic as exemplified by the reduced volume measurements and the reduced width and depth measurements [Table 2]. The borders, white matter landmarks and internal structure is much less distinct.

We found no difference in SN volume between controls and Parkinson's disease, but in progressive supranuclear palsy the volume was markedly reduced [Table 1]. This was in accord with the markedly thinned appearance of the SN in axial sections on MRI and pathology and increased Perls staining for iron [Fig. 5]. In Parkinson's disease the white matter landmarks and nigrosomes were still visible although the latter appeared less clearly defined; in progressive supranuclear palsy the topographical destruction was far greater. The undulation of the anterior border of the SN reported by Kwon et al. (2012) does not have an obvious pathological correlate particularly given that this is topographically likely to be part of the SNr as it is found in the most anterior and medial part of the whole SN.

Table 2
Anatomy of substantia nigra pars compacta (SNc) at level of red nucleus (RN) and exiting IIIrd nerve fascicles on histopathology.

SNc at the level of the RN and IIIrd nerve exit			Control			PSP			PD		
Histopathology			LFB	Perl	PV	LFB	Perl	PV	LFB	Perl	PV
Borders	Anterior	Medial blurring	3/3	3/3	3/3	2/2	2/2	2/2	2/2	2/2	2/2
		Lateral clarity	3/3	3/3	3/3	2/2	2/2	2/2	2/2	2/2	2/2
	Posterior	TMF	3/3	Mild 3/3	0/3	1/2	Mild 1/2	0/2	2/2	0/2	0/2
		ML	3/3	0/3	0/3	2/2	0/2	1/2 extn	2/2	0/2	0/2
	Medial	III	3/3	0/3	0/3	2/2	0/2	0/2	2/2	0/2	0/2
	Lateral	CC	3/3			3/3			3/3		
Landmarks	AM		3/3	2/3	2/3 hypo	2/2	2/2	Hypo	2/2	2/2	2/2 hypo
	AL		3/3	3/3	3/3 hypo	2/2	2/2	Hypo	2/2	2/2	Hypo
	PL		3/3	1/3	3/3	2/2	2/2	Hypo	2/2	2/2	Hypo
Internal anatomy	N1		3/3	3/3 hypo		Sparse/absent	Hyper++ 2/2		Absent	2/2 hypo	
	N2		2/3	2/3 hyper		Sparse/absent	Hyper++ 2/2		Sparse/absent	2/2 hyper	
	N3		3/3	2/3 hypo		Sparse/absent	Hypo		Absent	2/2 hypo	
	N4		3/3	3/3 hypo		Sparse/absent	Hyper++ 2/2		Sparse/absent	2/2 hypo	
	N5										
	Pincer		3/3	3/3 hypo		0/2	0/2		0/2	2/2	
	Hook		3/3	2/3 hyper		1/2	0/2		2/2	2/2	
Comments						Thin, streaky, high Perl stain			Thick, pale nigrosomes		

Table 3
Anatomy of substantia nigra pars compacta (SNc) at level of red nucleus (RN) and exiting IIIrd nerve fascicles on high field spin-echo MRI. Case 1 never had pathological examination and so was excluded from this part of the analysis.

SNc at the level of the RN and IIIrd nerve exit			Control		PSP		PD	
SE MRI images			LFB	SE MRI	LFB	SE MRI	LFB	SE MRI
Borders	Anterior	Medial blurring	9/9	9/9	8/8	8/8	5/5	5/5
		Lateral clarity	9/9	9/9	7/8	6/8	4/5	5/5
	Posterior	TMF	7/9	7/9	3/8	7/8	4/5	5/5
		ML	9/9	9/9	8/8	8/8	4/5	5/5
	Medial	III	9/9	9/9	8/8	8/8	4/5	5/5
	Lateral	CC	8/9	8/9	8/8	8/8	4/5	5/5
Landmarks	AM		7/9	8/9	7/8	5/8	4/5	4/5
	AL		9/9	9/9	8/8	5/8	5/5	5/5
	PL		9/9	8/9	6/8	1/8	5/5	5/5
Internal anatomy	N1		9/9	9/9	6/8 sparse	2/8 stringy	0/5	5/5 faint
	N2		9/9	0/9	6/8 sparse	0/8	4/5 sparse	0/5
	N3		9/9	7/9	6/8 sparse	1/8	3/5 sparse	3/5 faint
	N4		8/9	8/9	4/8 sparse	4/8 stringy	4/5 sparse	5/5 faint
	N5							
	Pincer		9/9	9/9	0/8	3/8	0/5	4/5
	Hook		6/9	9/9	5/8	2/8	5/5	5/5
Comments								

Use of post-mortem pathological specimens validates our findings on high field spin-echo MRI which was obtained without movement artifacts and time or tolerability constraints which limit *in vivo* acquisitions. However, the MRI characteristics including relaxation times of fixed post-mortem tissue at room temperature are different to those at body temperature *in vivo* and fixation leads to asymmetric tissue shrinkage (Quester and Schroder, 1997).

The anatomy of the SN is highly complex and as can be seen from the serial axial sections [Fig. 1] it varies in its cross sectional dimensions and the internal organisation throughout its course. Even the angle of histological sectioning may alter the appreciated anatomy (Gibb, 1992; McRitchie et al., 1995; McRitchie et al., 1996; Damier et al., 1999a, b; German et al., 1989; Fearnley and Lees, 1991; Gibb and Lees, 1991; Hassler, 1937; Olzewski, 1954). Currently, conventional imaging techniques are too insensitive to these subtleties possibly explaining the heterogeneity of published work (Adachi et al., 1999; Gorell et al., 1995; Martin et al., 2008; Savoiardo et al., 1994; Massey and Yousry, 2010), with pathological confirmation the exception rather than rule (Blazejewska et al., 2013; Oikawa et al., 2002). Many early studies have been based on a presumed understanding of the anatomy on conventional MRI (Duguid et al., 1986, Drayer, 1988a, b, Rutledge et al., 1987, Pujol et al., 1992) (for review see Massey and Yousry, 2010).

High resolution 3 T imaging sensitive to the paramagnetic effects of neuromelanin shows signal hyperintensity in the SN (Sasaki et al., 2006). Multishot diffusion-weighted MR imaging with a left to right diffusion direction gradient may better define the borders of the SN than T2w imaging (Adachi et al., 1999). Other published techniques to delineate the SN include T1 weighted techniques (Menke et al., 2009), relaxometry (Gorell et al., 1995; Martin et al., 2008; Ordidge et al., 1994; Peran et al., 2010), segmented inversion recovery imaging (Hutchinson et al., 2003; Raff et al., 2006), T2w and T2*-weighted techniques (Eapen et al., 2011), susceptibility weighted imaging (SWI) (Abosch et al., 2010) and magnetisation transfer ratio imaging (Helms et al., 2009).

More recent *in vivo* work at 7.0 T has improved the resolution, contrast and signal-to-noise ratio using T2* (Cho et al., 2011; Kwon et al., 2012) and at 3.0 T *in vivo* the swallow tail sign has been found to be a reliably identifiable feature in the dorsolateral SN (Schwarz et al., 2014; Reiter et al., 2015). However, caution is still required in interpreting imaging even at 3.0 T - the resolution of *in vivo* images remains below that required for accurate discrimination of these subdivisions in the SN. Diffusion tensor imaging has been shown to be both highly sensitive and specific for Parkinson's disease (Vaillancourt et al., 2009), and to demonstrate age-appropriate changes (Vaillancourt et al., 2012), although these findings have not been corroborated (Schwarz et al., 2013).

CB immunohistochemistry has enabled us to define nigrosomes on our histological sections (Damier et al., 1999a) with all 5 nigrosomes seen in serial axial MR images [Fig. 1]. We do not appear to be imaging the pigmented neurons themselves - when they are absent in Parkinson's disease the spin-echo MRI hyperintensity remains [Fig. 5]. This is in keeping with pathological work where the nigrosome structure is maintained even in the face of loss of pigmented SNc cells (Damier et al., 1999a, b). Many studies have tried to detect differences in the traditionally-defined SNc (Duguid et al., 1986) using conventional MRI. There are reports of reduced width (Duguid et al., 1986; Pujol et al., 1992; Braffman et al., 1989; Stern et al., 1989; Yagishita and Oda, 1996) or smudging of the SNr hypointensity (Savoiardo et al., 1994; Drayer, 1988a, b; Savoiardo et al., 1989; Savoiardo et al., 1990). However, only one study has found a correlation between the width of the SNc and a measure of clinical severity (Pujol et al., 1992).

Using multishot diffusion-weighted MRI to define the borders of the SN more clearly also did not show a reduced SN width in Parkinson's disease (Adachi et al., 1999), and there were similar findings using diffusion-weighted or fast STIR images (Oikawa et al., 2002). However, this is not greatly surprising as although there is loss of neuromelanin-containing pigmented cells in the SNc in Parkinson's disease (Fearnley and Lees, 1991; Ma et al., 1997; Hardman et al., 1997) the pathological literature supports the fact that the volume of the SN does not reduce in Parkinson's disease (Ma et al., 1997). In fact, pathological data in ageing (Cabello et al., 2002) and a recent imaging study in Parkinson's disease (Kwon et al., 2012) even suggest that it may paradoxically increase in size. Our data support this idea - both in terms of the absolute measured volume not being significantly different from controls in Parkinson's disease [Table 2], and in the appearance of the SN in the axial plane having preserved width and depth both subjectively [Fig. 5] and quantitatively [Table 2]. Although there has already been some success in detecting the regional distribution of pathology in the SN in Parkinson's disease using techniques sensitive to microscopic changes such as DTI (Peran et al., 2010; Vaillancourt et al., 2009; Chan et al., 2007) in agreement with the pathological topography (Fearnley and Lees, 1991), subsequent studies have not confirmed this (Menke et al., 2009).

In progressive supranuclear palsy far greater destruction of the borders and internal architecture of the SN is found with loss of the nigrosomal spin-echo MRI hyperintensity [Fig. 5, Tables 2 & 3]. This is manifest as a reduced volume which is consistent with both the pathological literature where progressive supranuclear palsy affects both SNr and SNc (Hardman et al., 1997; Oyanagi et al., 2001), and imaging literature where a smaller SN has been described using multishot diffusion-weighted imaging (Adachi et al., 1999). Many conventional MRI abnormalities have been described in the SN in progressive supranuclear palsy but none are of clinical utility currently (Massey et al., 2012a).

There remain many unanswered questions that will inform future research: there is very little information about the heterogeneity of iron deposition in the body and anterior border of the SN and the precise location of the iron, or its role in the pathogenesis. The precise anatomical correlate of signal hyperintensity on spin-echo MRI in the region of the nigrosomes is not clear but it appears not to be the pigmented neurons of the SNc as already discussed. The best method to study the anatomy of the SN is also unclear - iron is clearly important in the pathogenesis and so iron-sensitive techniques such as T2*-weighted MRI and SWI should be employed but we have shown that iron strays

outside the SN proper and therefore these methods may be misleading. Further studies are needed to answer some of these questions which in the absence of SN morphological changes in Parkinson's disease, will require quantitative MRI techniques such as relaxometry, DTI and MTI with higher than currently commonly available in-plane resolution, with correlative histopathological work.

We have demonstrated the anatomy of the SN histologically and applied this knowledge to understand the complex and heterogeneous high field spin-echo MRI SN appearance in the same tissue. We have demonstrated the visibility of the nigrosomes using this technique and the preservation of N1 in Parkinson's disease but not progressive supranuclear palsy, in accordance with pathological evidence. Further work is needed to clarify the pathological correlates of MRI findings.

Funding

LAM, HGP, MM and OA-H have all been supported by grants from the Progressive Supranuclear Palsy Association (Europe). MM has also been partially supported by AlBan, High Level Scholarship Programme of the European Union (2004–2006) and Caja de Seguro Social (CSS), Panama. This work was undertaken at UCLH/UCL who received a proportion of funding from the UK Department of Health's National Institute for Health Research Biomedical Research Centre's funding scheme (UCLH/UCL Comprehensive Biomedical Research Trust). The research was partly supported by the National Institute for Health Research (NIHR) Biomedical Research Unit in Dementia based at University College London Hospitals (UCLH), University College London (UCL).

Acknowledgements

We are indebted to the donors to the Queen Square Brain Bank for Neurological Disorders without whom this work would not have been possible. Part of this work has been presented and was awarded the junior award for excellence in clinical research at the 12th international congress of Parkinson's disease and movement disorders in Chicago in June 2008. The views expressed are those of the author(s) and not necessarily those of the NHS, the NIHR or the Department of Health.

References

Abosch, A., Yacoub, E., Ugurbil, K., Harel, N., 2010 Dec. An assessment of current brain targets for deep brain stimulation surgery with susceptibility-weighted imaging at 7 Tesla. Neurosurgery 67 (6), 1745–1756 (discussion 56).

Adachi, M., Hosoya, T., Haku, T., Yamaguchi, K., Kawanami, T., 1999 Sep. Evaluation of the substantia nigra in patients with Parkinsonian syndrome accomplished using multishot diffusion-weighted MR imaging. AJNR 20 (8), 1500–1506.

Blazejewska, A.I., Schwarz, S.T., Pitiot, A., Stephenson, M.C., Lowe, J., Bajaj, N., et al., 2013 Aug 6. Visualization of nigrosome 1 and its loss in PD: pathoanatomical correlation and in vivo 7 T MRI. Neurology 81 (6), 534–540.

Braffman, B.H., Grossman, R.I., Goldberg, H.I., Stern, M.B., Hurtig, H.I., Hackney, D.B., et al., 1989 Jan. MR imaging of Parkinson disease with spin-echo and gradient-echo sequences. AJR 152 (1), 159–165.

Cabello, C.R., Thune, J.J., Pakkenberg, H., Pakkenberg, B., 2002 Aug. Ageing of substantia nigra in humans: cell loss may be compensated by hypertrophy. Neuropathol. Appl. Neurobiol. 28 (4), 283–291.

Chan, L.L., Rumpel, H., Yap, K., Lee, E., Loo, H.V., Ho, G.L., et al., 2007 Dec. Case control study of diffusion tensor imaging in Parkinson's disease. J. Neurol. Neurosurg. Psychiatry 78 (12), 1383–1386.

Cho, Z.H., Oh, S.H., Kim, J.M., Park, S.Y., Kwon, D.H., Jeong, H.J., et al., 2011 Mar. Direct visualization of Parkinson's disease by in vivo human brain imaging using 7.0 T magnetic resonance imaging. Mov. Disord. 26 (4), 713–718.

Damier, P., Hirsch, E.C., Agid, Y., Graybiel, A.M., 1999 Auga. The substantia nigra of the human brain. I. Nigrosomes and the nigral matrix, a compartmental organization based on calbindin D(28K) immunohistochemistry. Brain 122 (Pt 8), 1421–1436.

Damier, P., Hirsch, E.C., Agid, Y., Graybiel, A.M., 1999 Augb. The substantia nigra of the human brain. II. Patterns of loss of dopamine-containing neurons in Parkinson's disease. Brain 122 (Pt 8), 1437–1448.

Drayer, B.P., 1988 Mara. Imaging of the aging brain. Part I. Normal findings. Radiology 166 (3), 785–796.

Drayer, B.P., 1988 Marb. Imaging of the aging brain. Part II. Pathologic conditions. Radiology 166 (3), 797–806.

Duguid, J.R., De La Paz, R., DeGroot, J., 1986 Dec. Magnetic resonance imaging of the midbrain in Parkinson's disease. Ann. Neurol. 20 (6), 744–747.

Eapen, M., Zald, D.H., Gatenby, J.C., Ding, Z., Gore, J.C., 2011 Apr. Using high-resolution MR imaging at 7 T to evaluate the anatomy of the midbrain dopaminergic system. AJNR Am. J. Neuroradiol. 32 (4), 688–694.

Fearnley, J.M., Lees, A.J., 1990 Dec. Striatonigral degeneration. A clinicopathological study. Brain 113 (Pt 6), 1823–1842.

Fearnley, J.M., Lees, A.J., 1991 Oct. Ageing and Parkinson's disease: substantia nigra regional selectivity. Brain 114 (Pt 5), 2283–2301.

German, D.C., Manaye, K., Smith, W.K., Woodward, D.J., Saper, C.B., 1989 Oct. Midbrain dopaminergic cell loss in Parkinson's disease: computer visualization. Ann. Neurol. 26 (4), 507–514.

Gibb, W.R., 1992 May 29. Melanin, tyrosine hydroxylase, calbindin and substance P in the human midbrain and substantia nigra in relation to nigrostriatal projections and differential neuronal susceptibility in Parkinson's disease. Brain Res. 581 (2), 283–291.

Gibb, W.R., Lees, A.J., 1991 May. Anatomy, pigmentation, ventral and dorsal subpopulations of the substantia nigra, and differential cell death in Parkinson's disease. J. Neurol. Neurosurg. Psychiatry 54 (5), 388–396.

Gibb, W.R., Fearnley, J.M., Lees, A.J., 1990. The anatomy and pigmentation of the human substantia nigra in relation to selective neuronal vulnerability. Adv. Neurol. 53, 31–34.

Gorell, J.M., Ordidge, R.J., Brown, G.G., Deniau, J.C., Buderer, N.M., Helpern, J.A., 1995 Jun. Increased iron-related MRI contrast in the substantia nigra in Parkinson's disease. Neurology 45 (6), 1138–1143.

Halliday, G.M., 2004. Chapter 14: substantia nigra and locus coeruleus. In: Paxinos, G., Mai, J.K. (Eds.), The Human Nervous System, second ed. 2004. Academic Press.

Hardman, C.D., Halliday, G.M., McRitchie, D.A., Cartwright, H.R., Morris, J.G., 1997 Mar. Progressive supranuclear palsy affects both the substantia nigra pars compacta and reticulata. Exp. Neurol. 144 (1), 183–192.

Hassler, R., 1937. Zur Normalanatomie der Substantia Nigra. Versuch einer architektonishen Gliederung. J. Psychol. Neurol. 48, 1–55.

Hassler, R., 1938. Zur Pathologie der Paralysis agitans und des Postenzephalitischen Parkinsonismus. J. Psychol. Neurol. 48, 387–476.

Helms, G., Draganski, B., Frackowiak, R., Ashburner, J., Weiskopf, N., 2009 Aug 1. Improved segmentation of deep brain grey matter structures using magnetization transfer (MT) parameter maps. NeuroImage 47 (1), 194–198.

Hutchinson, M., Raff, U., Lebedev, S., 2003 Nov. MRI correlates of pathology in parkinsonism: segmented inversion recovery ratio imaging (SIRRIM). NeuroImage 20 (3), 1899–1902.

Ince, P.G., Clarke, B., Holton, J.L., Revesz, T., Wharton, S., Love, S., Louis, D.N., Ellison, D.W., 2008. Disorders of movement and system degenerations. Greenfield's Neuropathology, eighth ed. 1, pp. 889–1030.

Kwon, D.H., Kim, J.M., Oh, S.H., Jeong, H.J., Park, S.Y., Oh, E.S., et al., 2012 Feb. Seven-tesla magnetic resonance images of the substantia nigra in Parkinson disease. Ann. Neurol. 71 (2), 267–277.

Ma, S.Y., Roytta, M., Rinne, J.O., Collan, Y., Rinne, U.K., 1997 Oct 3. Correlation between neuromorphometry in the substantia nigra and clinical features in Parkinson's disease using disector counts. J. Neurol. Sci. 151 (1), 83–87.

Mai, J.K., Stephens, P.H., Hopf, A., Cuello, A.C., 1986 Mar. Substance P in the human brain. Neuroscience 17 (3), 709–739.

Martin, W.R., Wieler, M., Gee, M., 2008 Apr 15. Midbrain iron content in early Parkinson disease: a potential biomarker of disease status. Neurology 70 (16 Pt 2), 1411–1417.

Massey, L.A., Yousry, T.A., 2010 Feb. Anatomy of the substantia nigra and subthalamic nucleus on MR imaging. Neuroimaging Clin. N. Am. 20 (1), 7–27.

Massey, L.A., Micallef, C., Paviour, D.C., O'Sullivan, S.S., Ling, H., Williams, D.R., et al., 2012 Deca. Conventional magnetic resonance imaging in confirmed progressive supranuclear palsy and multiple system atrophy. Mov. Disord. 27 (14), 1754–1762.

Massey, L.A., Miranda, M.A., Zrinzo, L., Al-Helli, O., Parkes, H.G., Thornton, J.S., et al., 2012 Feb 1b. High resolution MR anatomy of the subthalamic nucleus: imaging at 9.4 T with histological validation. NeuroImage 59 (3), 2035–2044.

McRitchie, D.A., Halliday, G.M., 1995 Mar. Calbindin D28k-containing neurons are restricted to the medial substantia nigra in humans. Neuroscience 65 (1), 87–91.

McRitchie, D.A., Halliday, G.M., Cartwright, H., 1995 Sep. Quantitative analysis of the variability of substantia nigra pigmented cell clusters in the human. Neuroscience 68 (2), 539–551.

McRitchie, D.A., Hardman, C.D., Halliday, G.M., 1996 Jan 1. Cytoarchitectural distribution of calcium binding proteins in midbrain dopaminergic regions of rats and humans. J. Comp. Neurol. 364 (1), 121–150.

Menke, R.A., Scholz, J., Miller, K.L., Deoni, S., Jbabdi, S., Matthews, P.M., et al., 2009 Aug 15. MRI characteristics of the substantia nigra in Parkinson's disease: a combined quantitative T1 and DTI study. NeuroImage 47 (2), 435–441.

Nieuwenhuys, R., Voogd, J., van Huijzen, C., 1988. The Human Central Nervous System: A Synopsis and Atlas 3rd Revised Edition.

Oikawa, H., Sasaki, M., Tamakawa, Y., Ehara, S., Tohyama, K., 2002 Nov–Dec. The substantia nigra in Parkinson disease: proton density-weighted spin-echo and fast short inversion time inversion-recovery MR findings. AJNR Am. J. Neuroradiol. 23 (10), 1747–1756.

Olzewski, J.B.D., 1954. Cytoarchitecture of the Human Brain Stem.

Ordidge, R.J., Gorell, J.M., Deniau, J.C., Knight, R.A., Helpern, J.A., 1994 Sep. Assessment of relative brain iron concentrations using T2-weighted and T2*-weighted MRI at 3 Tesla. Magn. Reson. Med. 32 (3), 335–341.

Oyanagi, K., Tsuchiya, K., Yamazaki, M., Ikeda, K., 2001 Apr. Substantia nigra in progressive supranuclear palsy, corticobasal degeneration, and parkinsonism-dementia complex of Guam: specific pathological features. J. Neuropathol. Exp. Neurol. 60 (4), 393–402.

Peran, P., Cherubini, A., Assogna, F., Piras, F., Quattrocchi, C., Peppe, A., et al., 2010 Nov. Magnetic resonance imaging markers of Parkinson's disease nigrostriatal signature. Brain 133 (11), 3423–3433.

Pujol, J., Junque, C., Vendrell, P., Grau, J.M., Capdevila, A., 1992 Nov. Reduction of the substantia nigra width and motor decline in aging and Parkinson's disease. Arch. Neurol. 49 (11), 1119–1122.
Quester, R., Schroder, R., 1997 Jul 18. The shrinkage of the human brain stem during formalin fixation and embedding in paraffin. J. Neurosci. Methods 75 (1), 81–89.
Raff, U., Hutchinson, M., Rojas, G.M., Huete, I., 2006 Jun. Inversion recovery MRI in idiopathic Parkinson disease is a very sensitive tool to assess neurodegeneration in the substantia nigra: preliminary investigation. Acad. Radiol. 13 (6), 721–727.
Rasbrand, W.S., 2009. Image J. US National Institutes of Health, Bethesda, Maryland, USA. http://rsb.info.gov/ij/.
Reiter, E., Mueller, C., Pinter, B., Krismer, F., Scherfler, C., Esterhammer, R., et al., 2015 Jul. Dorsolateral nigral hyperintensity on 3.0 T susceptibility-weighted imaging in neurodegenerative Parkinsonism. Mov. Disord. 30 (8), 1068–1076.
Rutledge, J.N., Hilal, S.K., Silver, A.J., Defendini, R., Fahn, S., 1987 Aug. Study of movement disorders and brain iron by MR. AJR 149 (2), 365–379.
Sasaki, M., Shibata, E., Tohyama, K., Takahashi, J., Otsuka, K., Tsuchiya, K., et al., 2006 Jul 31. Neuromelanin magnetic resonance imaging of locus coeruleus and substantia nigra in Parkinson's disease. Neuroreport 17 (11), 1215–1218.
Savoiardo, M., Strada, L., Girotti, F., D'Incerti, L., Sberna, M., Soliveri, P., et al., 1989 Jul–Aug. MR imaging in progressive supranuclear palsy and Shy-Drager syndrome. J. Comput. Assist. Tomogr. 13 (4), 555–560.
Savoiardo, M., Strada, L., Girotti, F., Zimmerman, R.A., Grisoli, M., Testa, D., et al., 1990 Mar. Olivopontocerebellar atrophy: MR diagnosis and relationship to multisystem atrophy. Radiology 174 (3 Pt 1), 693–696.
Savoiardo, M., Girotti, F., Strada, L., Ciceri, E., 1994. Magnetic resonance imaging in progressive supranuclear palsy and other parkinsonian disorders. J. Neural Transm. 42, 93–110.
Schwarz, S.T., Abaei, M., Gontu, V., Morgan, P.S., Bajaj, N., Auer, D.P., 2013. Diffusion tensor imaging of nigral degeneration in Parkinson's disease: a region-of-interest and voxel-based study at 3 T and systematic review with meta-analysis. NeuroImage Clin. 3, 481–488.
Schwarz, S.T., Afzal, M., Morgan, P.S., Bajaj, N., Gowland, P.A., Auer, D.P., 2014. The 'swallow tail' appearance of the healthy nigrosome - a new accurate test of Parkinson's disease: a case-control and retrospective cross-sectional MRI study at 3 T. PLoS One 9 (4), e93814.
Stern, M.B., Braffman, B.H., Skolnick, B.E., Hurtig, H.I., Grossman, R.I., 1989 Nov. Magnetic resonance imaging in Parkinson's disease and parkinsonian syndromes. Neurology 39 (11), 1524–1526.
Trojanowski, J.Q., Revesz, T., 2007 Dec. Proposed neuropathological criteria for the post mortem diagnosis of multiple system atrophy. Neuropathol. Appl. Neurobiol. 33 (6), 615–620.
Vaillancourt, D.E., Spraker, M.B., Prodoehl, J., Abraham, I., Corcos, D.M., Zhou, X.J., et al., 2009 Apr 21. High-resolution diffusion tensor imaging in the substantia nigra of de novo Parkinson disease. Neurology 72 (16), 1378–1384.
Vaillancourt, D.E., Spraker, M.B., Prodoehl, J., Zhou, X.J., Little, D.M., 2012 Jan. Effects of aging on the ventral and dorsal substantia nigra using diffusion tensor imaging. Neurobiol. Aging 33 (1), 35–42.
Yagishita, A., Oda, M., 1996 May. Progressive supranuclear palsy: MRI and pathological findings. Neuroradiology 38 (Suppl. 1), S60–S66.
Yushkevich, P.A., Piven, J., Hazlett, H.C., Smith, R.G., Ho, S., Gee, J.C., Gerig, G., 2006. User-guided 3D active contour segmentation of anatomical structures: significantly improved efficiency and reliability. Neuroimage 31 (3), 1116–1128 (Jul. 1).